

Supplementary Information

Carboxylic ligands to enhance material recovery from construction waste to produce CaCO_3 for carbon utilization

Jonah M. Williams^{1,2}, Diandian Zhao^{2,3}, Ning Zhang^{1,2}, Shiho Kawashima^{2,3}, and Aaron J. Moment^{4,*}

¹Department of Earth and Environmental Engineering, Columbia University, New York, New York, 10027

²Lenfest Center for Sustainable Energy, Columbia University, New York, New York, 10027

³Department of Civil Engineering and Engineering Mechanics, Columbia University, New York, New York, 10027

⁴Department of Materials Science and Engineering, University of California Los Angeles, Los Angeles, CA, 90095

* ajmoment@seas.ucla.edu

Table S1. Overall material balance, acid utilized, and elemental recoveries for Ca, Si, Fe, and Al for each carboxylate ligand used.

	mol Ca / mol organic salt	mol Si / mol organic salt	mol Fe / mol organic salt	mol Al / mol organic salt	Ca recovery (g Ca / g Ca in feedstock)	Si recovery (g Si / g Si in feedstock)	Fe recovery (g Fe / g Fe in feedstock)	Al recovery (g Al / g Al in feedstock)
Control	-	-	-	-	0.704	0.11	0.05	0.75
Sodium Glutamate	1.547	0.141	0.002	0.069	0.703	0.14	0.03	0.69
Sodium Formate	1.567	0.201	0.008	0.113	0.712	0.20	0.10	1.00
Sodium Acetate	1.580	0.205	0.008	0.108	0.718	0.21	0.09	1.00
Sodium Citrate	1.584	0.406	0.037	0.124	0.720	0.40	0.44	1.00

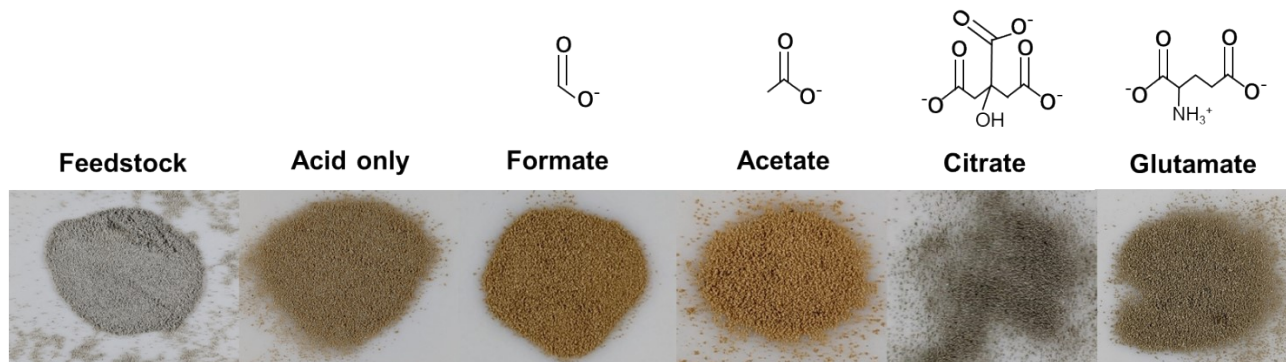


Figure S1. Visual images of the PERR recovered from the leaching reactor for HCl only (control), formate, acetate, citrate, and glutamate leaching cases. Images compared to the original waste hydrated cement paste (HCP) feedstock on the left.

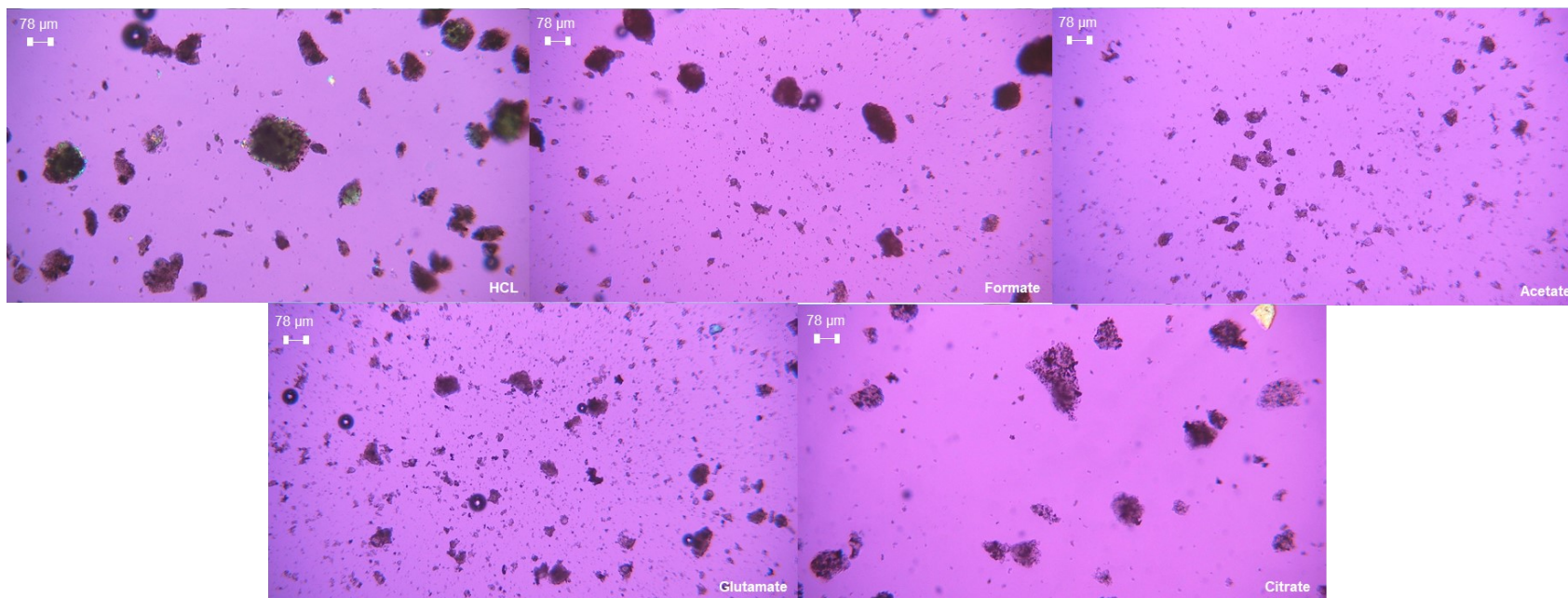


Figure S2. Optical microscopy at 10x showing the morphology of the post-extraction reactor residue (PERR) for the control and four ligands utilized during leaching.

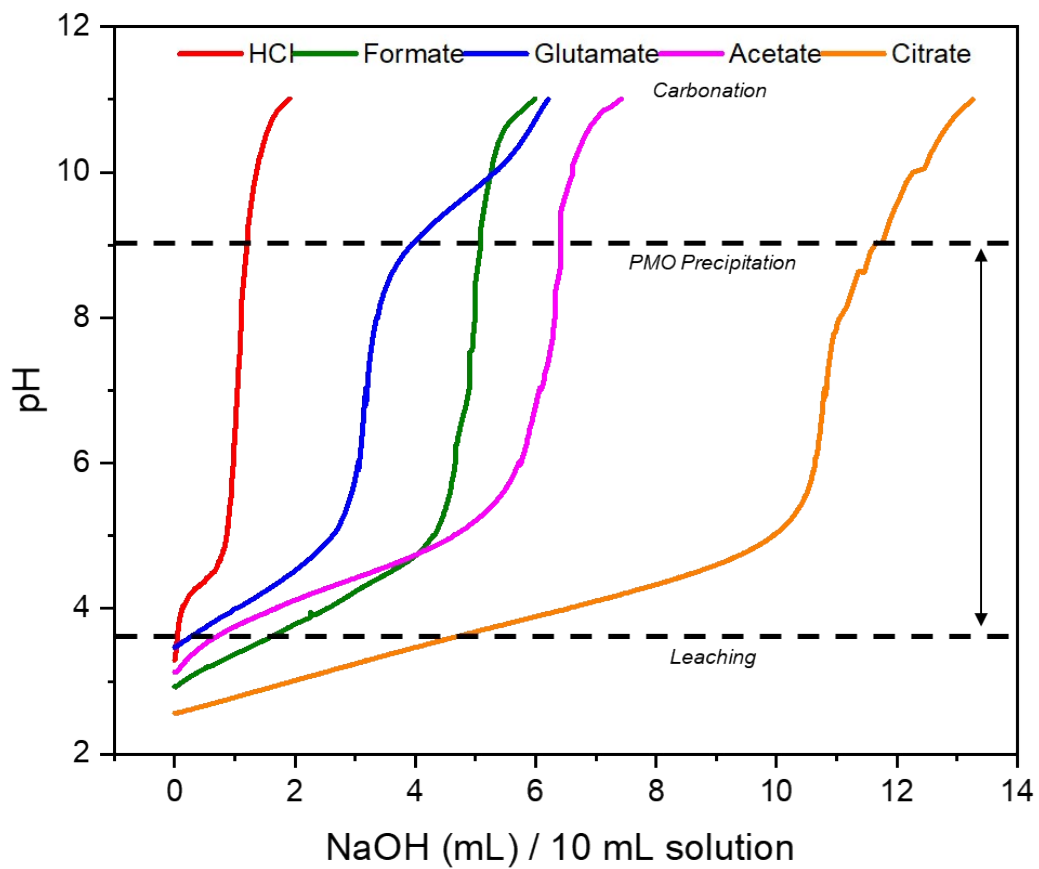


Figure S3. Titration curves as obtained by the auto titration unit for the five leachate solutions as their pH was raised from acidic to basic for carbonation.

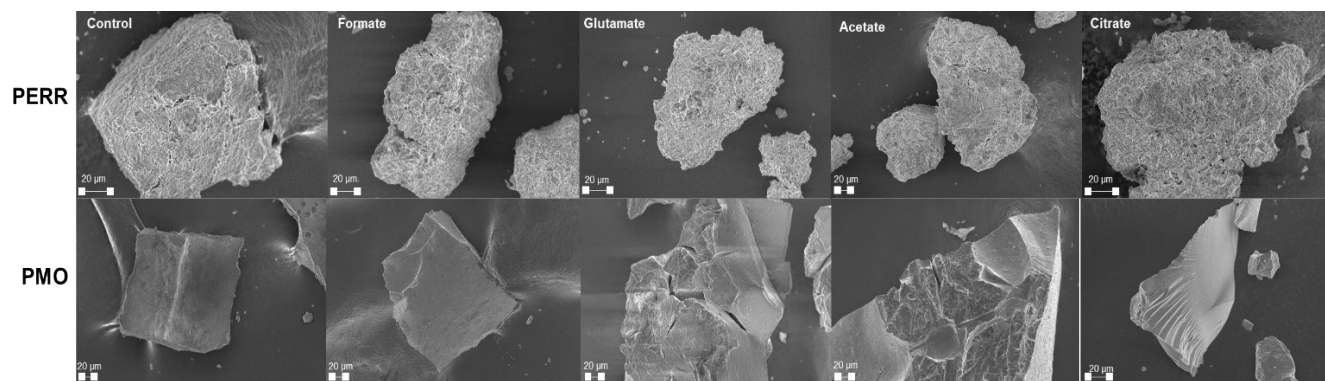


Figure S4. SEM images of the produced PERR and PMO showing the distinct morphologies between the two.

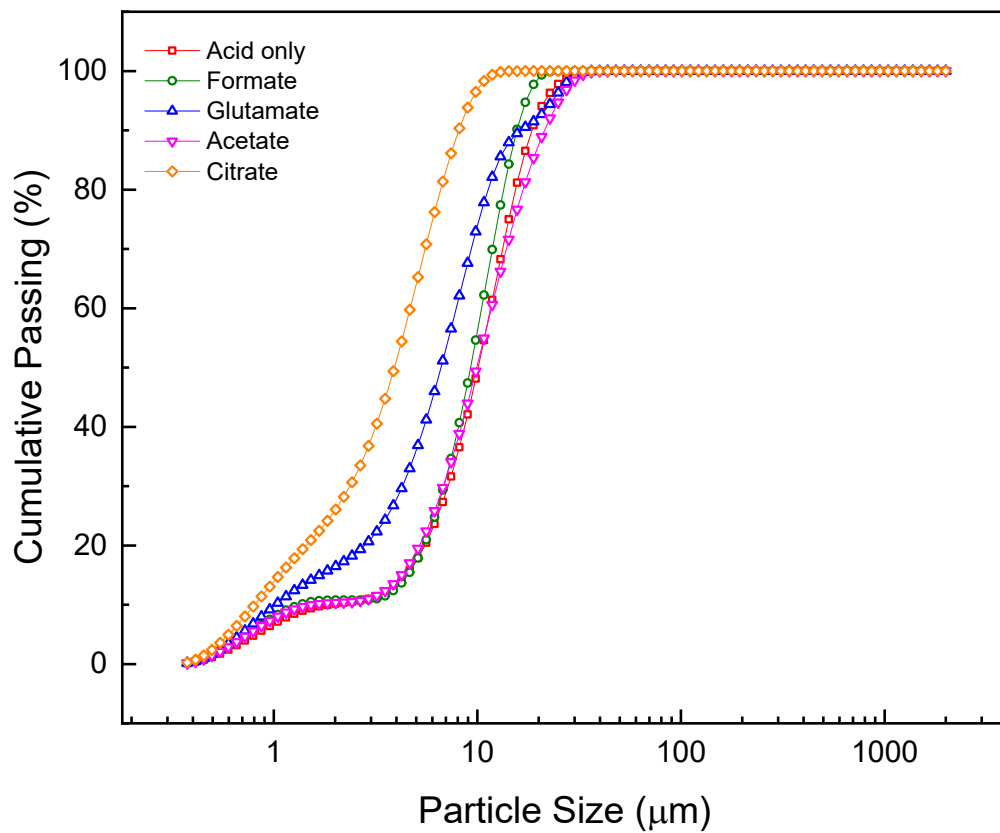


Figure S5. PSD data for the calcium carbonates produced from the carboxylic-assisted leaching processes displayed in cumulative passing (%).

Table S2. Carbonate crystalline phase as determined by Rietveld refinement and carbon balance

Case	Calcite (%)	Vaterite (%)	Aragonite (%)	Carbonate Yield (% , without PMO swing)	Carbonate Yield (% , with PMO swing)
HCl	52.7	47.3	0	~100	87
Formate	66.8	33.2	0	~100	62
Acetate	90.1	9.9	0	~100	58
Glutamate	6.0	94.0	0	~100	57
Citrate	17.8	82.2	0	96	42

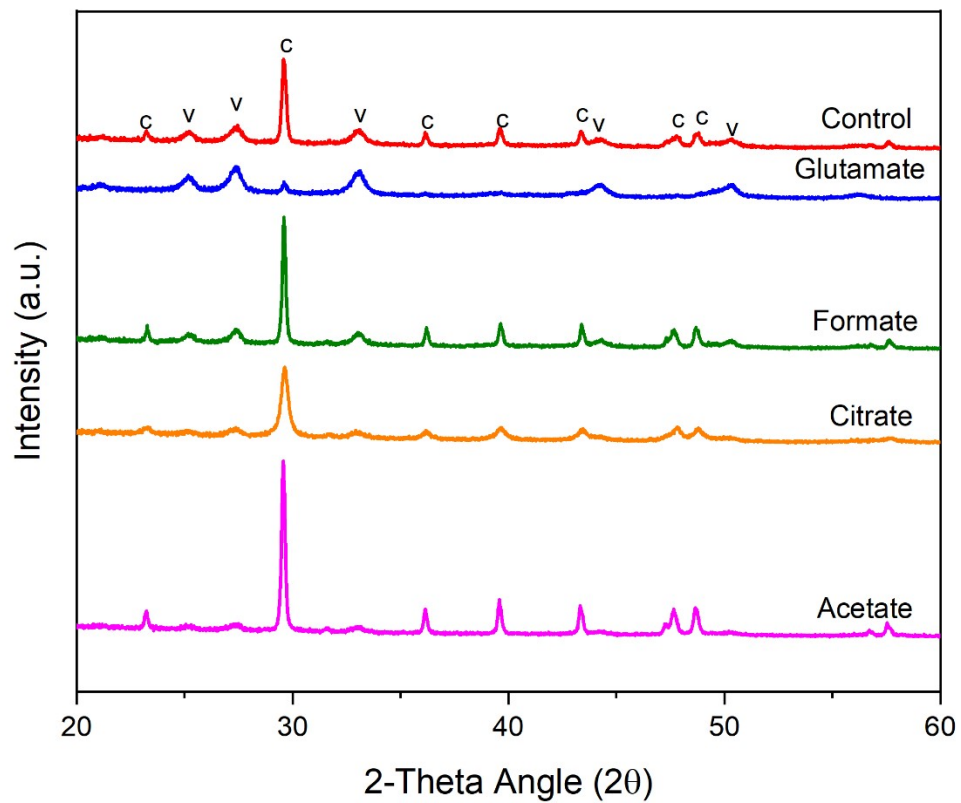


Figure S6. P-XRD data for the produced calcium carbonate samples. C indicates major calcite peaks while v indicated major vaterite peaks. No aragonite was detected at the crystallization conditions utilized.